HSE abundance and size (Fig. 3B). This observation suggests that in reduced bodies, late-accreted metal was predominantly added to the core, whereas in oxidized bodies, such as Mars, Earth, and the angrite parent body, metal was substantially mixed into the mantle. This is a logical consequence of the higher ferric iron contents of oxidized bodies, because ferric iron provides the potential for the oxidation of metal and its dissolution in mantle silicates (*6, 30*). During the principal phase of metallic core formation, all bodies were saturated in metal and hence highly reduced. Oxidation is believed to have occurred through the addition of more-oxidized materials toward the end of accretion (*31*). In the cases of Earth and Mars, there was an additional mechanism for the production of ferric iron through the disproportionation of ferrous iron into ferric iron plus Fe metal (*32, 33*). This mechanism requires the stabilization of silicate perovskite at very high pressures in the lower mantle, a process that occurs widely on Earth, to a small extent on Mars, and not at all in smaller bodies.

It appears that late accretion was spatially and temporally widespread in the inner solar system, with HSE abundances in differentiated asteroids and the terrestrial planets reflecting both the extent of initial removal into the metallic core and the proportion of material added by late accretion. If the oxidation state exerted the dominant control on HSE abundances in the silicate mantles of all bodies, including the Moon, it follows then that the oxidizing conditions of the silicate mantles of Earth and Mars were established before, or synchronously with, late accretion, although not necessarily at the conditions seen at the present day.

References and Notes

1. A. Borisov, H. Palme, B. Spettel, *Geochim. Cosmochim. Acta* **58**, 705 (1994).
2. W. Ertel, H. S. O'Neill, P. J. Sylvester, D. B. Dingwell, *Geochim. Cosmochim. Acta* **63**, 2439 (1999).
3. H. Becker *et al.*, *Geochim. Cosmochim. Acta* **70**, 4528 (2006).
4. A. D. Brandon, R. J. Walker, J. W. Morgan, C. G. Goles, *Geochim. Cosmochim. Acta* **64**, 4083 (2000).
5. J. H. Jones, C. R. Neal, J. C. Ely, *Chem. Geol.* **196**, 21 (2003).
6. K. Kimura, R. S. Lewis, E. Anders, *Geochim. Cosmochim. Acta* **38**, 683 (1974).
7. K. Righter, M. Humayun, L. Danielson, *Nat. Geosci.* **1**, 321 (2008).
8. V. R. Murthy, *Science* **253**, 303 (1991).
9. W. Ertel, M. J. Walter, M. J. Drake, P. J. Sylvester, *Geochim. Cosmochim. Acta* **70**, 2591 (2006).
10. J. M. Brenan, W. F. McDonough, *Nat. Geosci.* **2**, 798 (2009).
11. A. Holzheid, P. Sylvester, H. S. C. O'Neill, D. C. Rubie, H. S. Palme, *Nature* **406**, 396 (2000).
12. R. J. Walker, *Chemie Erde-Geochem.* **69**, 101 (2009).
13. C.-L. Chou, *Lunar Planet. Sci. Conf.* **IX**, 219 (1978).
14. Alternative models to explain the HSE contents of the silicate mantles of Earth, Mars, and the Moon include reduced sequestering of HSE by metal at high temperatures and pressures and inefficient core formation. The former scenario is not supported by current data. Furthermore, adequate convergence of partition coefficients for all HSEs at high temperature and pressure seems unlikely. Inefficient core formation, whereby solid or liquid metal is retained in the mantle during core formation, can account for any given siderophile element concentration according to the precise proportion of solid and liquid metal retained. The differing compatibility of HSEs in liquid and solid metal, however, will lead to HSE fractionation by this process. It is also difficult to account for the concentrations of other siderophile and chalcophile elements such as Ni, Co, and S by any one set of parameters (*12*).
15. J. M. D. Day, D. G. Pearson, L. A. Taylor, *Science* **315**, 217 (2007).
16. J. M. D. Day, R. J. Walker, O. B. James, I. S. Puchtel, *Earth Planet. Sci. Lett.* **289**, 595 (2010).
17. W. F. Bottke, R. J. Walker, J. M. D. Day, D. Nesvorny, L. Elkins-Tanton, *Science* **330**, 1527 (2010).
18. T. Kleine *et al.*, *Geochim. Cosmochim. Acta* **73**, 5150 (2009).
19. R. C. Greenwood, I. A. Franchi, A. Jambon, P. C. Buchanan, *Nature* **435**, 916 (2005).
20. A. Morbidelli, W. F. Bottke, D. Nesvorny, H. F. Levison, *Icarus* **204**, 558 (2009).
21. Materials and methods are available in the supplementary materials; analyses were performed following techniques described previously.
22. E. R. D. Scott, R. C. Greenwood, I. A. Franchi, I. S. Sanders, *Geochim. Cosmochim. Acta* **73**, 5835 (2009).
23. There is less fractionation of Pt, Pd, and Re from Os, Ir, and Ru during partial mantle melting on Vesta and the Moon than on Earth (Fig. 2). This is most likely due to the differing oxygen and sulfur fugacities on these parent bodies, which will affect the partitioning of HSEs between mantle minerals and melts, and also, more importantly, affect the stability of phases that control the HSE budget. For example, metal exists at the oxygen fugacities present in the lunar and vestan mantles, but not in Earth's upper mantle.
24. J. L. Birck, C. J. Allegre, *Earth Planet. Sci. Lett.* **124**, 139 (1994).
25. After correction, some of the basaltic meteorite samples preserve very high HSE abundances, namely Johnstown (diogenite), Dhofar 007 (eucrite), and NWA2999 (angrite). It is possible that these high HSE concentrations reflect genuine abundances in the mantle of their parent body, implying substantial compositional heterogeneity. However, each of these meteorites contains an anomalously high proportion of metal [*34*, *35*); up to 10% for NWA2999], as compared to the <0.5% expected from equilibrium crystallization (*36*), and has high Ni content, suggesting that each has been affected by impact disturbance after, not before, igneous crystallization. It is also notable that the actual measured HSE proportions in each of these samples are chondritic, with no interelement variation that would be expected in either the residue or products of partial melting.
26. Previous data for HEDs suggested greater HSE heterogeneity in their parent body (*37*), but the relative uniformity of concentrations measured here suggests that at least some of that variation may be due to postcrystallization meteoritic contamination. Using the covariation of $^{187}Os/^{188}Os$ and Os concentration from previous preliminary data for angrites (*38*), we attain a parent body HSE concentration estimate that is indistinguishable from that presented here.
27. A. Borisov, H. Palme, *Geochim. Cosmochim. Acta* **59**, 481 (1995).
28. W. D. Maier *et al.*, *Nature* **460**, 620 (2009).
29. It has been suggested that angrites were derived from a much larger body than inferred from the short time scale of core formation (*18*). For the Moon, it might be argued that if the lunar impactor, thought to make up ~80% of the Moon [*39*) and references therein], was already differentiated and depleted, then the formation of the lunar core may have further removed HSEs from its mantle.
30. D. J. Frost, U. Mann, Y. Asahara, D. C. Rubie, *Philos. Trans. R. Soc. London Ser. A* **366**, 4315 (2008).
31. F. Albarède, *Nature* **461**, 1227 (2009).
32. J. Wade, B. J. Wood, *Earth Planet. Sci. Lett.* **236**, 78 (2005).
33. D. J. Frost *et al.*, *Nature* **428**, 409 (2004).
34. R. J. Floran *et al.*, *Geochim. Cosmochim. Acta* **45**, 2385 (1981).
35. M. Humayun, A. J. Irving, S. M. Kuehner, *Lunar Planet. Sci. Conf.* **XXXVIII**, 1221 (2007).
36. M. B. Duke, *J. Geophys. Res.* **70**, 1523 (1965).
37. R. J. Walker *et al.*, *Lunar Planet. Sci. Conf.* **XLII**, 1386 (2011).
38. A. J. V. Riches, J. M. D. Day, R. J. Walker, Y. Liu, L. A. Taylor, *Lunar Planet. Sci. Conf.* **XLII**, 2288 (2011).
39. R. M. Canup, E. Asphaug, *Nature* **412**, 708 (2001).
40. E. Anders, N. Grevesse, *Geochim. Cosmochim. Acta* **53**, 197 (1989).
41. M. Wadhwa, in *Oxygen in the Solar System,* G. J. MacPherson, D. W. Mittlefehldt, J. H. Jones, S. B. Simon, Eds. (Mineralogical Society of America and Geochemical Society, Washington DC, 2008), vol. 68, pp. 493–510.
42. D. Canil, *Nature* **389**, 842 (1997).
43. D. Trail, E. B. Watson, N. D. Tailby, *Nature* **480**, 79 (2011).

Acknowledgments: We are grateful to the Natural History Museum, London, for the provision of numerous samples. C.W.D. acknowledges funding from grant NER/C51902X/1 from the Natural Environment Research Council, UK. We thank three anonymous referees for their constructive comments and H. Williams for useful discussions. Full HSE and Os isotope data are available in the supplementary materials.

Supplementary Materials

www.sciencemag.org/cgi/content/full/336/6077/72/DC1
Materials and Methods
Supplementary Text
Figs. S1 to S4
Table S1
References (*44*–*85*)

7 October 2011; accepted 2 March 2012
10.1126/science.1214967

Mapping the Core of the *Arabidopsis* Circadian Clock Defines the Network Structure of the Oscillator

W. Huang,[1] P. Pérez-García,[1] A. Pokhilko,[2] A. J. Millar,[2,3] I. Antoshechkin,[4] J. L. Riechmann,[1,4,5] P. Mas[1]*

In many organisms, the circadian clock is composed of functionally coupled morning and evening oscillators. In *Arabidopsis*, oscillator coupling relies on a core loop in which the evening oscillator component TIMING OF CAB EXPRESSION 1 (TOC1) was proposed to activate a subset of morning-expressed oscillator genes. Here, we show that TOC1 does not function as an activator but rather as a general repressor of oscillator gene expression. Repression occurs through TOC1 rhythmic association to the promoters of the oscillator genes. Hormone-dependent induction of *TOC1* and analysis of RNA interference plants show that TOC1 prevents the activation of morning-expressed genes at night. Our study overturns the prevailing model of the *Arabidopsis* circadian clock, showing that the morning and evening oscillator loops are connected through the repressing activity of TOC1.

The molecular circuitry underlying circadian rhythms relies on the reciprocal regulation of clock components forming negative-feedback loops at the core of the oscillator (*1*). However, deciphering the oscillator transcriptional regulatory code is a major challenge

due to the interplay among clock activators and repressors, which are responsible for the generation of the loops. In *Arabidopsis*, two MYB transcription factors, CIRCADIAN CLOCK ASSOCIATED 1 (CCA1) and LATE ELONGATED HYPOCOTYL (LHY) (*2*, *3*)—together with the pseudoresponse regulators PRR5, 7, and 9 (*4*)—function as key components of a so-called "morning loop," which interlocks with an evening loop (*5*, *6*) composed of TIMING OF CAB EXPRESSION 1 (TOC1) (or PRR1) (*4*, *7*), GIGANTEA (GI) (*8*, *9*), and a hypothetical component Y (*10*). The evening loop also includes the evening complex composed of EARLY FLOWERING 3 and 4 (ELF3 and ELF4), as well as LUX ARRHYTHMO (LUX) (*11*, *12*).

Regulation of TOC1 rhythmic expression is essential for proper functioning of the clock (*13*, *14*). Mechanisms that contribute to this regulation include changes in chromatin structure (*15*), transcriptional regulation (*16*), and protein degradation (*17*). Alterations of this regulation affect clock function and result in disrupted circadian gene expression and changes in time to flower (*7*, *18*, *19*). TOC1 also connects environmental signals with clock-controlled photomorphogenic and hormonal outputs (*18*, *20*). Gene expression analysis using *toc1* mutant plants led to the hypothesis that TOC1 inhibits its expression by activating the repressors CCA1 and LHY (*16*, *21*). The direct interaction of TOC1 with CCA1 HIKING EXPEDITION was proposed as a regulatory link connecting TOC1 with the activation of *CCA1* (*21*). Our study changes the sign of TOC1 function at the core of the clock and shows that the morning and evening feedback loops are connected through the repressing activity of TOC1.

We used chromatin immunoprecipitation followed by deep sequencing (ChIP-Seq) to obtain a high-resolution map of TOC1 chromatin occupancy on a genome-wide scale (*22*). The ChIP experiments were performed with TOC1 minigene (TMG) seedlings expressing the genomic fragment of *TOC1* fused to the yellow fluorescent protein (*18*) in the *toc1-2* (hypomorphic mutant) background (fig. S1) (*7*). ChIP-Seq data analysis in search of genes that contained one or more TOC1 binding regions identified 867 peak-to-gene associations (ChIP-Seq peak P value ≤ 0.001) corresponding to 772 potential TOC1 target genes (fig. S2 and table S1). Consistent with previous studies (*20*, *21*), we found that *CCA1* and *ABAR*/*CHLH*/*GUN5*, binding targets of TOC1, were present in our gene list. The *ABAR* circadian expression is repressed by TOC1 (*20*).

As TOC1 is a key component of the *Arabidopsis* circadian system, we analyzed the proportion of TOC1-binding genes that were under the control of the circadian clock. Using different circadian gene expression data sets (*23*, *24*), we found that 40% of TOC1 targets were regulated by the circadian clock (figs. S3 and S4 and tables S1, S2, and S6). Analysis of peak phases of expression revealed a phase enrichment around dawn (Fig. 1, A to C, and table S3), which suggests that TOC1 modulates clock genes expressed during the morning phase. We also found that the promoters of the oscillator components were occupied by TOC1. The targets included genes from both the morning (*CCA1*, *LHY*, *PRR9*, and *PRR7*) and evening loops (*GI*, *TOC1*, *ELF4*, and *LUX*) (Fig. 1, D to G, and table S4). We also identified other components associated to the oscillator such as *PRR5* (*13*), whereas other clock-related genes more indirectly linked to the transcriptional regulation of the oscillator—such as *ZTL*, *FKF1*, or *LKP2* (*13*) or clock genes expressed only in specific tissues (e.g., *PRR3*) (*13*)—were not found as putative TOC1 targets. Independent ChIP–quantitative polymerase chain reaction (QPCR) analyses showed specific amplification of the regions identified by ChIP-Seq, consistent with the binding of TOC1 to the promoters of the oscillator genes (fig. S5). We further validated our results by using TOC1-overexpressing plants (TOC1-ox), in which TOC1 is constitutively expressed. In these plants, TOC1 occupancy at the oscillator loci was significantly higher than occupancy at the promoters of genes not present in our ChIP-Seq list (fig. S5). We therefore report the association of TOC1 to the promoters of the morning and evening oscillator genes. Binding might be indirect and may require other cofactors and/or the formation of higher-order protein complexes.

Analysis of TOC1-bound oscillator sequences identified a significantly enriched motif closely related to the GBox (named GBox-expanded) (Fig. 1H, fig. S6, and table S5). We also found that a motif very similar to the circadian motif, evening element (EE), was present in both morning- and evening-expressed oscillator genes (named EE-like–expanded) (Fig. 1I and fig. S6). The EE motif was proposed to be associated with evening-expressed genes (*16*, *25*). The motifs were positioned

[1]Center for Research in Agricultural Genomics, Barcelona 08193, Spain. [2]School of Biological Sciences, University of Edinburgh, Edinburgh EH9 3JH, UK. [3]Centre for Systems Biology at Edinburgh, C. H. Edinburgh EH9 3JD, UK. [4]California Institute of Technology, Division of Biology, Pasadena, CA 91125, USA. [5]Institució Catalana de Recerca i Estudis Avançats, Barcelona 08010, Spain.

*To whom correspondence should be addressed. E-mail: paloma.mas@cragenomica.es

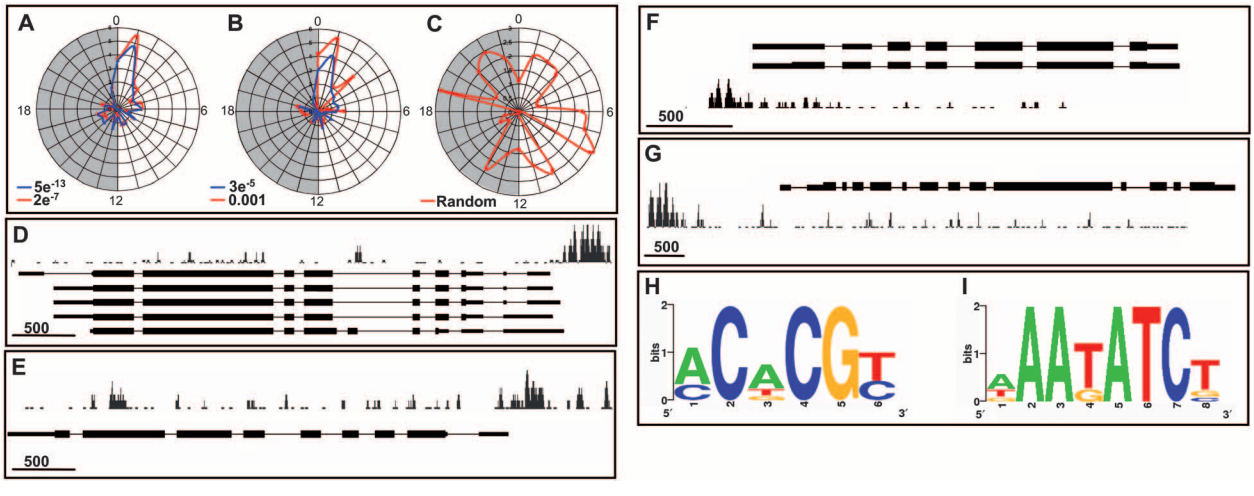

Fig. 1. Analysis of TOC1 ChIP-Seq circadian targets. Global trend of expression phases within TOC1 circadian targets (**A** and **B**) and for a random list of circadian genes (**C**). Phase enrichments were graphically portrayed within a range of ChIP-Seq P values at different Zeitgeber times (radial axis: 0-dawn; 12-dusk). The white and gray areas represent day and night, respectively. Peak traces of *LHY* (**D**), *PRR7* (**E**), *PRR9* (**F**), and *GI* (**G**) from TOC1 ChIP-Seq data. The exon-intron–untranslated region structure of the different gene models above and below each panel indicates forward and reverse orientation, respectively. Position weight matrix representation of consensus motifs present within the TOC1 target oscillator sequences. The Gbox-expanded (**H**) and EE-like–expanded (**I**) motifs were identified using the *SCOPE* motif finder. Both strands were used to compute the significance value. ChIP-Seq, peak visualization, circadian phase analysis, and motif discovery were performed as described in the supporting online material (SOM).

very close to the center of the TOC1-bound ChIP-Seq genomic regions (fig. S6). A similar positional enrichment at the peak maximum was observed when sequences of the circadian genes bound by TOC1 were analyzed (fig. S6). The results were consistent with a ChIP-QPCR screening of the *CCA1* promoter, showing that amplicon enrichment decreased as the distance from the GBox and EE-like motifs increased (fig. S6).

We next analyzed the role of the circadian clock in modulating TOC1 interaction with its target genes by performing ChIP assays with TMG plants synchronized under 12-hours light/12-hours dark (LD) cycles. The results revealed a rhythmic oscillation of TOC1 binding with a peak at Zeitgeber time 15 (ZT15, 3 hours after lights off; ZT0, lights on), the proposed time of TOC1 function (Fig. 2, A to D). Similar oscillatory binding was observed in plants grown under constant light (LL) conditions (Fig. 2, E and F), indicating a role for the circadian clock. The rhythmicity was abolished in TOC1-ox plants (Fig. 2, G and H), suggesting that TOC1 binding is dictated by its protein abundance, which is under circadian regulation. These results, together with the arrhythmic phenotypes of TOC1-ox (*18*), support the notion that the circadian pattern of TOC1 binding is relevant for TOC1 function in the clock.

We next examined oscillator gene expression in wild-type (WT) and TOC1-ox samples under LD and LL cycles. The peak expression of transcripts from the morning-loop genes (*PRR9*, *PRR7*, *CCA1*, and *LHY*) was significantly reduced in TOC1-ox (Fig. 2, I and J, fig. S7, and table S7). This is noteworthy, as TOC1 was previously assumed to be an activator of *CCA1* and *LHY* expression (*16*). The reduced expression cannot be attributed to the activation of their known repressors PRR7 and PRR9, as their expression is also decreased in TOC1-ox plants. Analysis of the evening loop also revealed gene repression. For instance, *GI* and *ELF4* were reduced around dusk (Fig. 2, K and L), and plants expressing the *LUX* promoter fused to *LUCIFERASE* (*LUX::LUC*) also displayed a reduced promoter activity, particularly during the night (fig. S8). In the morning loop, oscillator components that are expressed at a similar phase repress each other's expression (e.g., CCA1 and LHY) (*2*, *3*). Our results suggest that similar regulation occurs in the evening loop, where TOC1 might also repress genes expressed during the night. The observed function of TOC1 as a repressor is not likely due to constitutive overexpression of TOC1, as we also observed decreased oscillator expression in TMG plants (expressing *TOC1* under its own promoter) (Fig. 2, I to L).

To further confirm the transcriptional repressing function of TOC1, we generated transgenic plants expressing TOC1 fused to the GR domain of the glucocorticoid receptor (*26*). In the absence of a steroid ligand, the GR domain retains a nuclear factor in the cytoplasm, but nuclear localization is restored in the presence of the synthetic glucocorticoid dexamethasone (Dex). Treatment of TOC1-GR plants with Dex resulted in a reduction of *CCA1* and *GI* expression relative to the mock-treated controls (Fig. 3, A and B, and fig. S9). Our analysis revealed statistically significant differences between TOC1-GR+Dex and the other genotypes (±Dex) (Fig. 3, D and E), whereas no significant variations were found in WT plants in the presence or absence of Dex. We also analyzed the effects of TOC1-GR induction by Dex on *CCA1::LUC* activity. The in vivo studies were consistent with the reverse transcription QPCR data and showed a clear reduction of *CCA1::LUC* luminescence in Dex-treated plants (Fig. 3C). To further address the repressing function of TOC1, we examined *CCA1* expression in TOC1-GR plants treated with Dex in the presence or absence of the protein synthesis inhibitor cycloheximide (CHX). Our results showed that *CCA1* expression was reduced after Dex treatment in the presence of CHX (Fig. 3F), indicating that *CCA1* repression does not require de novo protein synthesis. We also used the previously described induction of *TOC1* by the plant hormone abscisic acid (ABA) (*20*). We analyzed *TOC1* induction by ABA and, in parallel, we examined *CCA1* and *PRR9* expression. The results showed that the induction of *TOC1* was accompanied by a concomitant reduction of *CCA1* and *PRR9* expression (Fig. 3, G to I). Together with the results from *toc1* mutant plants (Fig. 4), our studies indicate that, in contrast to its previously assigned activating role, TOC1 functions as a repressor of oscillator gene expression.

The repressive function of TOC1 provides an explanation for recently published experimental data that cannot be reconciled with an activating role for TOC1. For instance, analysis of *ztl* mutant plants, with increased TOC1 accumulation (*17*), revealed a reduced expression of *LHY* and *CCA1* (*27*), which is not consistent with TOC1 activating function. The data also showed low

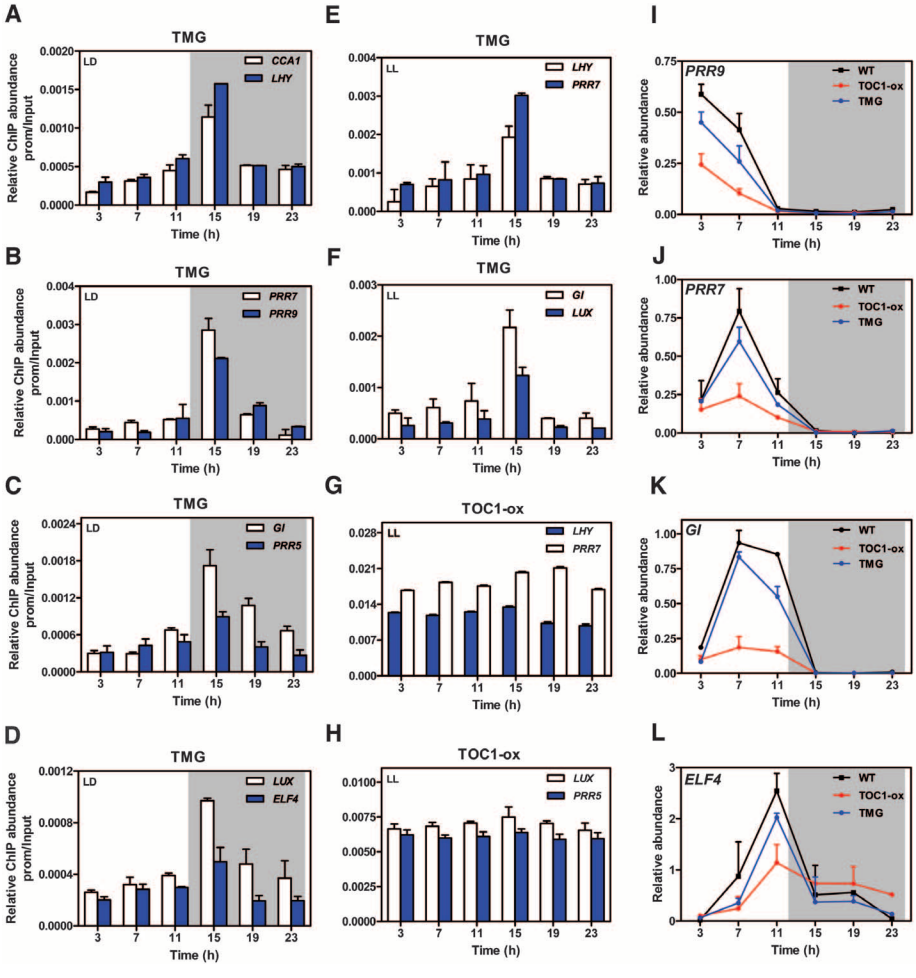

Fig. 2. TOC1 binds to the promoters of the oscillator genes and inhibits their expression. ChIP-QPCR assays of TMG plants that were sampled every 4 hours over a 24-hour LD cycle are shown. Primers encompassing target sequences obtained in the ChIP-Seq analysis were used to amplify *CCA1* and *LHY* (**A**), *PRR7* and *PRR9* (**B**), *GI* and *PRR5* (**C**), or *LUX*/*PCL1* and *ELF4* (**D**). Binding was also examined under LL conditions following entrainment in TMG (**E** and **F**) and in TOC1-ox plants (**G** and **H**). Values are represented as means ± SEM. Expression profiling of *PRR9* (**I**), *PRR7* (**J**), *GI* (**K**), and *ELF4* (**L**) in WT, TMG, and TOC1-ox plants. Gene expression was analyzed in plants grown under LD cycles. mRNA abundance was normalized to *IPP2* expression. Values represent means ± SEM. White shading, day; gray shading, night.

abundance of *PRR9* and *PRR7* expression (*27*). Thus, the reduced expression of *LHY* and *CCA1* cannot be attributed to increased abundance of their inhibitors. To clarify TOC1 function in the clock, we examined oscillator gene expression in TOC1 RNA interference (RNAi) and *toc1-2* mutant plants grown under LD cycles. Our results showed an advanced phase for *LHY* expression at the onset of transcription (Fig. 4A and fig. S10), suggesting that the absence of TOC1 alleviates the repression normally observed in WT plants around dusk. The advanced phase of *LHY* expression correlated with a slight increase of *PRR7* (Fig. 4B and fig. S10). These results suggest that TOC1 temporally extends the repressing function of the other sequentially expressed PRR inhibitors (Fig. 4E) (*28*). The absence of TOC1 in *toc1* mutant plants shortens the duration of this repression, and as a consequence, the onset of *LHY* transcription is advanced (Fig. 4F). The effects on the trough of *LHY* are subtle, most likely because the expression of other *CCA1*/*LHY* repressors is also increased (Fig. 4, C and D). In TOC1-ox, the abnormally high expression of TOC1 during the day reveals its repressing function at times when TOC1 is not normally expressed (Fig. 4G). Altogether, our studies support the repressing function of TOC1 on oscillator gene expression, which changes the regulatory circuit at the core of the *Arabidopsis* circadian clock (fig. S11).

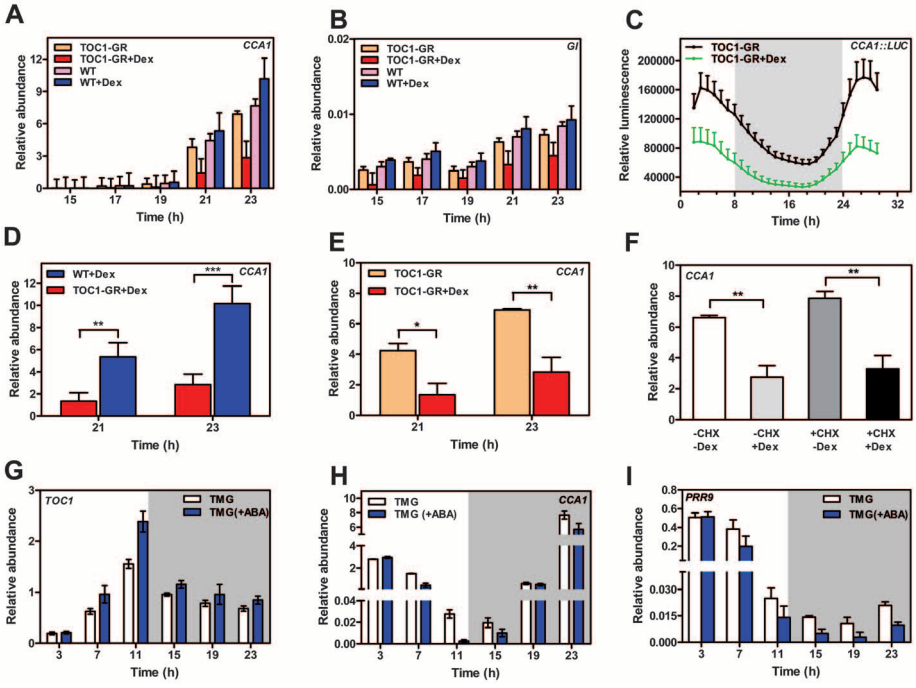

Fig. 3. Effects of TOC1 transient induction on oscillator gene expression. Analysis of *CCA1* (**A**) and *GI* (**B**) in WT and TOC1-GR plants mock-treated or treated with 5 μM dexamethasone (+Dex). Seedlings were treated at ZT10, and samples were analyzed at the indicated ZT. (**C**) Analysis of *CCA1::LUC* luminescence in TOC1-GR seedlings under 8-hours light/16-hours dark cycles. Luminescence was recorded 24 hours after the seedlings were transferred to a medium containing 5 μM of Dex. Data are presented as means ± SEM of luminescence signals from six to seven independent plants. (**D** to **F**) Comparisons of *CCA1* expression in TOC1-GR plants mock-treated or treated with 5 μM of Dex at ZT10 and analyzed at ZT21 and ZT23 in the absence (-CHX) or presence (+CHX) of 50 μM of cycloheximide. The statistical relevance of the differences is presented (*$P < 0.05$; **$P < 0.01$; ***$P < 0.001$). (**G** to **I**) Time-course analysis of *TOC1*, *CCA1*, and *PRR9* expression over the diurnal cycle in TMG plants in the presence or absence of the hormone ABA. Seedlings were sprayed with 100 μM (±) ABA at ZT5. The *y* axes of the *CCA1* and *PRR9* graphs were divided into segments so that repression at trough can clearly be observed. White shading, day; gray shading, night.

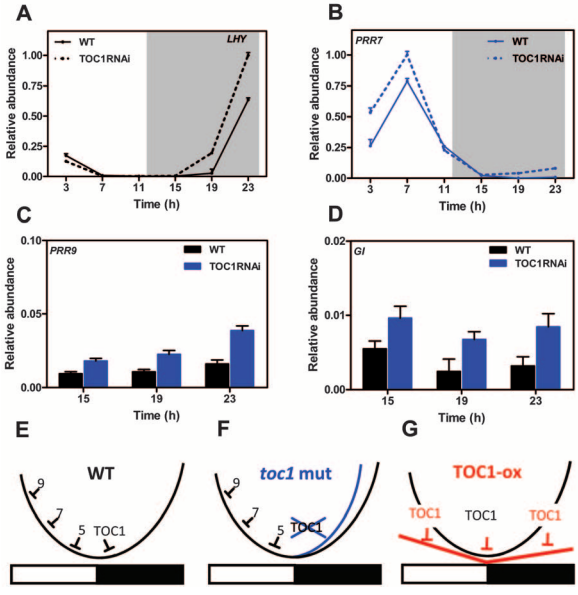

Fig. 4. Gene expression analysis in TOC1 RNAi plants. Analysis of *LHY* (**A**) and *PRR7* (**B**) expression under 12-hours light:12-hours dark conditions. Gene expression analysis of *PRR9* (**C**) and *GI* (**D**) during the night in TOC1 RNAi under 12-hours light/12-hours dark conditions. Values are represented as means ± SEM. Analysis was performed as described in the SOM. Schematic diagrams depicting the waveform of *CCA1/LHY* expression and the different waves of PRRs repression. Schemes depict the regulations in the wild type (black line) (**E**), *toc1* mutant (blue line), (**F**) and TOC1-ox (red line) (**G**). The small lines ending in perpendicular dashes represent repression. White boxes, day; black boxes, night.

Conclusions about the circadian transcriptional networks are complicated by the existence of multiple feedback loops and gene redundancies. Our study shows the complex and dynamic function of TOC1 as a regulator of oscillator gene expression, with a repressing activity of the morning and evening loops. Binding of TOC1 to the promoters of the oscillator genes may antagonize transcriptional activation around the time of peak expression. The mechanisms of oscillator gene activation are largely unknown, but chromatin remodeling and light-dependent regulation may play key roles at defined times of day. The challenge remains now to identify the mechanisms and components responsible for the activation of oscillator gene expression.

References and Notes

1. H. Wijnen, M. W. Young, *Annu. Rev. Genet.* **40**, 409 (2006).
2. R. Schaffer *et al.*, *Cell* **93**, 1219 (1998).
3. Z. Y. Wang, E. M. Tobin, *Cell* **93**, 1207 (1998).
4. A. Matsushika, S. Makino, M. Kojima, T. Mizuno, *Plant Cell Physiol.* **41**, 1002 (2000).
5. J. C. W. Locke *et al.*, *Mol. Syst. Biol.* **1**, article 2005.0013 (2005).
6. M. N. Zeilinger, E. M. Farre, S. R. Taylor, S. A. Kay, F. J. Doyle, *Mol. Syst. Biol.* **2**, 1 (2006).
7. C. A. Strayer *et al.*, *Science* **289**, 768 (2000).
8. S. Fowler *et al.*, *EMBO J.* **18**, 4679 (1999).
9. D. H. Park *et al.*, *Science* **285**, 1579 (1999).
10. A. Pokhilko *et al.*, *Mol. Syst. Biol.* **6**, 1 (2010).
11. D. A. Nusinow *et al.*, *Nature* **475**, 398 (2011).
12. E. Herrero *et al.*, *Plant Cell* (2012).
13. C. R. McClung, R. A. Gutiérrez, *Curr. Opin. Genet. Dev.* **20**, 588 (2010).
14. P. Más, *Trends Cell Biol.* **18**, 273 (2008).
15. M. Perales, P. Más, *Plant Cell* **19**, 2111 (2007).
16. D. Alabadí *et al.*, *Science* **293**, 880 (2001).
17. P. Más, W. Y. Kim, D. E. Somers, S. A. Kay, *Nature* **426**, 567 (2003).
18. P. Más, D. Alabadí, M. J. Yanovsky, T. Oyama, S. A. Kay, *Plant Cell* **15**, 223 (2003).
19. D. E. Somers, A. A. R. Webb, M. Pearson, S. A. Kay, *Development* **125**, 485 (1998).
20. T. Legnaioli, J. Cuevas, P. Mas, *EMBO J.* **28**, 3745 (2009).

21. J. L. Pruneda-Paz, G. Breton, A. Para, S. A. Kay, *Science* **323**, 1481 (2009).
22. Materials and methods are available as supporting material on *Science* Online.
23. M. F. Covington, J. N. Maloof, M. Straume, S. A. Kay, S. L. Harmer, *Genome Biol.* **9**, R130 (2008).
24. S. P. Hazen *et al.*, *Genome Biol.* **10**, R17 (2009).
25. T. P. Michael *et al.*, *PLoS Genet.* **4**, e14 (2008).
26. A. M. Lloyd, M. Schena, V. Walbot, R. W. Davis, *Science* **266**, 436 (1994).
27. A. Baudry *et al.*, *Plant Cell* **22**, 606 (2010).
28. N. Nakamichi *et al.*, *Plant Cell* **22**, 594 (2010).

Acknowledgments: We thank E. Meyerowitz for comments on the manuscript, E. Centeno for help with ChIP-Seq analysis, O. Casagran for help with the microfluidic arrays, M. Perales for help with the ChIP, L. Rico for help with the inducible constructs, and L. Schaeffer and D. Trout (Jacobs Genetics and Genomics Laboratory at Caltech) for the primary sequence data processing. This work was supported by grants to P.M. from the Ramón Areces Foundation, the Spanish Ministry of Science and Innovation (MICINN), the European Molecular Biology Organization (EMBO) Young Investigators Program, and from the European Heads of Research Councils and the European Science Foundation through the European Young Investigator Award; to J.L.R. from the European Comission (EC) Marie Curie program and MICINN; and to A.J.M. and others from the EC FP7 Collaborative Project TiMet. The Centre for Systems Biology at Edinburgh is a Centre for Integrative and Systems Biology supported by the Biotechnology and Biological Sciences Research Council and the Engineering and Physical Sciences Research Council award D019621. W.H. is supported by a Juan de la Cierva contract (MICINN) and P.P.-G. by a Formación de Personal Investigador fellowship (MICINN). Sequencing data have been deposited with the National Center for Biotechnology Information Gene Expression Omnibus under accession number GSE35952.

Supporting Online Material

www.sciencemag.org/cgi/content/full/science.1219075/DC1
Materials and Methods
SOM Text
Figs. S1 to S11
Tables S1 to S7
References (*29*–*45*)

12 January 2012; accepted 27 February 2012
Published online 8 March 2012;
10.1126/science.1219075

A Major Genome Region Underlying Artemisinin Resistance in Malaria

Ian H. Cheeseman,[1] Becky A. Miller,[2] Shalini Nair,[1] Standwell Nkhoma,[1] Asako Tan,[2] John C. Tan,[2] Salma Al Saai,[1] Aung Pyae Phyo,[3] Carit Ler Moo,[3] Khin Maung Lwin,[3] Rose McGready,[3,4,5] Elizabeth Ashley,[3,4,5] Mallika Imwong,[4] Kasia Stepniewska,[4,5,7] Poravuth Yi,[8] Arjen M. Dondorp,[4,5] Mayfong Mayxay,[6] Paul N. Newton,[5,6] Nicholas J. White,[4,5] François Nosten,[3,4,5] Michael T. Ferdig,[2] Timothy J. C. Anderson[1]*

Evolving resistance to artemisinin-based compounds threatens to derail attempts to control malaria. Resistance has been confirmed in western Cambodia and has recently emerged in western Thailand, but is absent from neighboring Laos. Artemisinin resistance results in reduced parasite clearance rates (CRs) after treatment. We used a two-phase strategy to identify genome region(s) underlying this ongoing selective event. Geographical differentiation and haplotype structure at 6969 polymorphic single-nucleotide polymorphisms (SNPs) in 91 parasites from Cambodia, Thailand, and Laos identified 33 genome regions under strong selection. We screened SNPs and microsatellites within these regions in 715 parasites from Thailand, identifying a selective sweep on chromosome 13 that shows strong association ($P = 10^{-6}$ to 10^{-12}) with slow CRs, illustrating the efficacy of targeted association for identifying the genetic basis of adaptive traits.

Artemisinin-based combination therapies (ACTs) are the first-line treatment in nearly all malaria-endemic countries (*1*) and are central to the current success of global efforts to control and eliminate *Plasmodium falciparum* malaria (*2*). Resistance to artemisinin (ART) in *P. falciparum* has been confirmed in Southeast Asia (*3*), raising concerns that it will spread to sub-Saharan Africa, following the path of chloroquine and anti-folate resistance (*4*). ART resistance results in reduced parasite clearance rates (CRs) after treatment (Fig. 1A) and is principally due to parasite genetics, which determines 58 and 64% of the variance in parasite CRs in western Cambodia and western Thailand, respectively (*5*, *6*). The resistance mechanism is unknown, but reduced killing of "ring"-stage parasites (*7*) and quiescence have been implicated (*8*). The genetic basis is likely to be simple. A single mutation in the *ubp1* gene confers ART resistance in the *P. chabaudi* mouse malaria model (*9*). Similarly, resistance to other antimalarials in *P. falciparum* involves single major-gene effects or is oligogenic (*10*).

Cross-population genomic comparisons offer a means to identify putative targets of natural selection (*11*–*14*). Targeted association analyses of genome regions under selection can then be used to directly identify the genetic basis of adaptive traits (*13*, *14*), minimizing the multiple-testing penalties constraining standard genome-wide association studies. We compared three neighboring Southeast Asian *P. falciparum* populations (in Laos, Thailand, and Cambodia) with low levels of genetic differentiation (Fig. 1B), but differences in CRs after ART treatment (Fig. 1C), to detect recent selective sweeps that may underlie resistance. Parasites from Laos are cleared rapidly (*15*) [median –log(CR) = 1; half-life of parasite decline = 2 hours], parasites from western Cambodia clear slowly [median –log(CR) 2.15, half-life 6 hours], and parasites from western Thailand show a wide range of clearance [median –log(CR) 1.4, half-life 3 hours]. CR distributions are significantly different between all locations (Thai-Cambodia, $D = 0.58$, $P < 0.001$; Thai-Laos, $D = 0.68$, $P < 0.001$; Cambodia-Laos, $D = 0.93$, $P < 0.001$; two-sided Kolmogorov-Smirnov test).

We genotyped 91 genetically unique single-clone parasites (27 from Laos, 30 from Cambodia, and 34 from Thailand) by hybridization to a custom Nimblegen genotyping array that scores single-nucleotide polymorphisms (SNPs) [1 SNP per 500 base pairs (bp)] and copy number variation (CNV) (*16*, *17*). Principal-components analysis (PCA) and global fixation indices (F_{ST}) confirmed low but significant differentiation between the three populations (Fig. 1, B and D). We characterized CNV across the three populations, identifying 78 common CNVs [minor allele frequency (MAF) > 5%] containing 209 genes (*17*).

For each SNP (MAF > 5%, $n = 6969$), we calculated two statistics to identify genome regions under strong selection for our three populations, measuring differentiation in haplotype structure [XP-EHH (*18*)] and allele frequency (F_{ST}) and classifying selected regions using a 10-kb sliding window approach (*17*) (Fig. 2 and fig. S1). Thirty-three nonoverlapping regions, comprising 2.4% of the 23-Mb genome, showed evidence for selection (top 1% of genome-wide values in both tests) in one or more populations and were ranked by the proportion of significant tests (table S1).

Known antimalarial resistance genes accounted for 10 out of 33 (10/33) genome regions. Three genes (*pfcrt, dhps,* and *dhfr*) were identified directly, whereas *GTP-cyclohydrolase I* showed evidence of selection within 5 kb (Fig. 2B). *pfmdr1* was not identified, most likely because the amplicon containing *pfmdr1* has multiple origins (*19*). An additional 23 genome regions showed strong signatures of selection (table S1 and fig. S1). Three regions, on chromosomes (chrs) 6, 13, and 14, were significant at multiple adjacent windows and ranked eighth, first, and second, respectively (table S1 and Fig. 2C). We did not observe evidence for selection at two proposed candidate loci, *atpase6* (Fig. 2A) (*20*) or *Part (21)*. Two

[1]Texas Biomedical Research Institute, San Antonio, TX 78245, USA. [2]The Eck Institute for Global Health, Department of Biological Sciences, University of Notre Dame, Notre Dame, IN 46556, USA. [3]Shoklo Malaria Research Unit, Mae Sot, Tak, Thailand. [4]Faculty of Tropical Medicine, Mahidol University, Bangkok, Thailand. [5]Centre for Tropical Medicine, Churchill Hospital, Oxford, UK. [6]Wellcome Trust–Mahosot Hospital–Oxford Tropical Medicine Research Collaboration, Mahosot Hospital, Vientiane, Lao People's Democratic Republic. [7]Worldwide Antimalarial Resistance Network, Oxford, UK. [8]The National Center for Parasitology, Entomology, and Malaria Control, Phnom Penh, Cambodia.

*To whom correspondence should be addressed. E-mail: tanderso@txbiomedgenetics.org

Mapping the Core of the *Arabidopsis* Circadian Clock Defines the Network Structure of the Oscillator

W. Huang, P. Pérez-García, A. Pokhilko, A. J. Millar, I. Antoshechkin, J. L. Riechmann and P. Mas

Science **336** (6077), 75-79.
DOI: 10.1126/science.1219075originally published online March 8, 2012

Tic TOC1 Plant Clock

The molecular clocks intertwined with cellular physiology regulate daily cycles. In plants, these circadian rhythms affect processes as diverse as carbon metabolism and leaf orientation. **Huang *et al.*** (p. 75, published online 8 March) have now analyzed the interactions driven by a key element of the circadian clock in plants, TOC1 ("TIMING OF CAB EXPRESSION 1"). TOC1 helps to coordinate responses of the morning and evening cycles, functioning to repress activity of other clock components.